nature COMMUNICATIONS

ARTICLE

Received 25 May 2015 | Accepted 26 Aug 2015 | Published 19 Oct 2015

DOI: 10.1038/ncomms9476 OPEN

Purely organic electroluminescent material realizing 100% conversion from electricity to light

Hironori Kaji[1], Hajime Suzuki[1], Tatsuya Fukushima[1], Katsuyuki Shizu[1,2], Katsuaki Suzuki[1], Shosei Kubo[1], Takeshi Komino[2], Hajime Oiwa[1], Furitsu Suzuki[1], Atsushi Wakamiya[1], Yasujiro Murata[1] & Chihaya Adachi[2,3,4]

Efficient organic light-emitting diodes have been developed using emitters containing rare metals, such as platinum and iridium complexes. However, there is an urgent need to develop emitters composed of more abundant materials. Here we show a thermally activated delayed fluorescence material for organic light-emitting diodes, which realizes both approximately 100% photoluminescence quantum yield and approximately 100% up-conversion of the triplet to singlet excited state. The material contains electron-donating diphenylamino-carbazole and electron-accepting triphenyltriazine moieties. The typical trade-off between effective emission and triplet-to-singlet up-conversion is overcome by fine-tuning the highest occupied molecular orbital and lowest unoccupied molecular orbital distributions. The nearly zero singlet–triplet energy gap, smaller than the thermal energy at room temperature, results in an organic light-emitting diode with external quantum efficiency of 29.6%. An external quantum efficiency of 41.5% is obtained when using an out-coupling sheet. The external quantum efficiency is 30.7% even at a high luminance of 3,000 cd m^{-2}.

[1] Institute for Chemical Research, Kyoto University, Uji, Kyoto 611-0011, Japan. [2] Center for Organic Photonics and Electronics Research, Kyushu University, 744 Motooka, Nishi, Fukuoka 819-0395, Japan. [3] JST, ERATO, Adachi Molecular Exciton Engineering Project. [4] International Institute for Carbon Neutral Energy Research (WPI-I2CNER), Kyushu University, 744 Motooka, Nishi, Fukuoka 819-0395, Japan. Correspondence and requests for materials should be addressed to H.K. (email: kaji@scl.kyoto-u.ac.jp) or to C.A. (email: adachi@opera.kyushu-u.ac.jp).

Electroluminescence (EL) was initially studied for fundamental interest[1–3]. Tang and VanSlyke[4] subsequently applied EL in organic light-emitting diodes (OLEDs), obtaining an external EL quantum efficiency (EQE) of 1% for a double-layer fluorescent OLED. OLEDs have since been studied extensively, with particular focus on increasing their efficiency in display and lighting applications. EQE (η_{EQE}) is the product of the internal quantum efficiency (IQE) and light out-coupling factor (η_{out}), $\eta_{EQE} = IQE \times \eta_{out}$. η_{out} is typically 20–30% (refs 5–8). IQE is obtained from $IQE = \beta \times \gamma \times \Phi_{PL}$, where β is the exciton generation factor resulting in photons, γ is the carrier balance ratio of holes and electrons, and Φ_{PL} is the photoluminescence (PL) quantum yield (PLQY). Singlet and triplet excitons are theoretically generated in a 1:3 ratio by electronic excitation[3]. Triplet excitons typically dissipate as heat rather than being converted into photons. Because only singlet excitons generate photons, the resulting β for fluorescent OLEDs is limited to 25%. Even under conditions where γ and Φ_{PL} are 100%, the theoretical maximum η_{EQE} of the resulting OLED is only 5–7.5%.

Increasing β and η_{out} are therefore important challenges to maximize EQE. β can be increased directly using triplet excitons. The heavy-atom effect can convert triplet excitons into phosphorescence. Intersystem crossing (ISC) involves transition from the singlet to triplet state, and can theoretically result in 100% of excitons being extracted as photons. The EQE of the first device based on such a concept in 1998 was 4% (ref. 9), and subsequently reached 19% in 2001 (ref. 10). EQEs exceeding 20% are now frequently reported for optimized devices incorporating well-designed materials[11]. However, phosphorescent materials for OLEDs are currently restricted to Pt and Ir complexes, which have limited availability and are expensive.

Triplet excitons can also potentially be exploited by reverse ISC (RISC), which involves transition from the lowest energy triplet state (T_1) to the lowest excited singlet state (S_1)[12–16]. Converting triplet excitons to singlet excitons allows all excitons to be used to generate photons. This strategy has typically not been effective, because S_1 is at a much higher energy than T_1. Spin inversion is also required for this transition. However, fabrications of efficient OLEDs based on RISC have been attempted in recent years[17–21]. Unlike normal fluorescence, the fluorescence resulting from triplet–singlet transition is delayed, so we term it thermally activated delayed fluorescence (TADF).

TADF occurs by two successive processes, shown in Fig. 1a as green arrows; RISC from T_1 to S_1, and subsequent radiative decay from S_1 to the ground state (S_0). RISC is effective when the energy difference between S_1 and T_1 (ΔE_{ST}) is small. The theoretical background (Supplementary Note 1) reveals that small ΔE_{ST} is achieved by separating highest occupied molecular orbital (HOMO) and lowest unoccupied molecular orbital (LUMO) distributions. However, this HOMO–LUMO separation decreases the oscillator strength (f) between S_1 and S_0, which lowers PLQY[21].

Here we report an organic TADF material, 9-[4-(4,6-diphenyl-1,3,5-triazin-2-yl)phenyl]-*N*,*N*,*N*′,*N*′-tetraphenyl-9*H*-carbazole-3,6-diamine, named DACT-II (Fig. 1b). DACT-II consists of electron-donating diphenylaminocarbazole and electron-accepting triphenyltriazine moieties, chemically bonded at a torsion angle α (Fig. 1b). We will demonstrate that both nearly zero ΔE_{ST}, which is smaller than the thermal energy at room temperature, and large f, resulting in a PLQY of 100%, are simultaneously achieved by precisely controlling the HOMO and LUMO distributions (Fig. 1c and Supplementary Fig. 1, the geometries were optimized at the PBE0/6-31G(d) level[22,23] using the Gaussian 09 software package[24]), although the two factors are considered to be in a trade-off relationship. The small ΔE_{ST} and large f of DACT-II allow 'all injected holes and electrons to be used in fluorescence', resulting in an IQE of 100%. **DACT-II-based OLEDs** exhibit a maximum EQE of 29.6% in the absence of out-coupling treatment, indicating an IQE of ~100%. The only loss of quantum efficiency in the device is via light out-coupling. A maximum EQE of 41.5% is obtained simply using an out-coupling sheet. Importantly, DACT-II also allows the typical substantial decrease in EQE with increasing luminance (efficiency roll-off) to be overcome. In DACT-II, S_1 and T_1 excitons are rapidly converted to photons because of its large f and small ΔE_{ST}. The rapid removal of both S_1 and T_1 excitons in the optimized DACT-II-based OLEDs suppresses triplet–triplet annihilation (TTA) and singlet–triplet annihilation, which are an origin of roll-off. Very high EQE up to 30.7% is achieved at 3,000 cd m^{-2}.

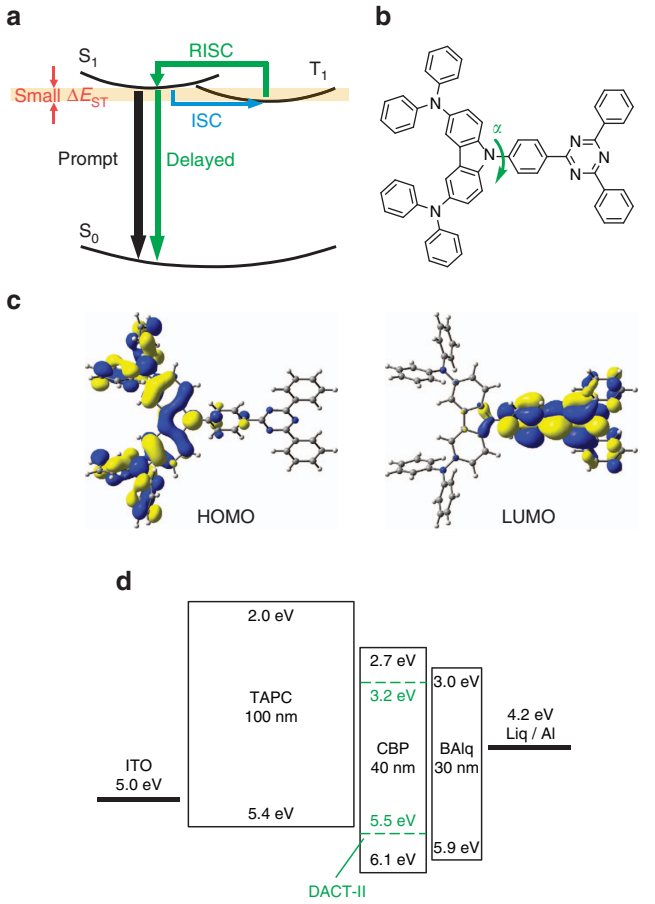

Figure 1 | DACT-II. (**a**) Schematic illustration of the TADF process. (**b**) Structure of DACT-II. (**c**) HOMO and LUMO distributions in DACT-II calculated at the PBE0/6-31G(d) level of theory. (**d**) Device structure and energy band diagram of **DACT-II-*x* OLEDs**. For the **DACT-II-100 OLED**, the EML consisted of DACT-II without CBP. Energy band diagrams of the reference fluorescent and phosphorescent OLEDs and other **DACT-II-*x* OLEDs** are shown in Supplementary Fig. 4.

Results

Organic light-emitting diodes. DACT-II, which consists only of C, H and N, was synthesized as described in Supplementary Note 2 and Supplementary Fig. 2. DACT-II has favourable thermal properties, with melting and decomposition temperatures of 266 °C and 484 °C, respectively. The sublimation temperature under vacuum was 308 °C. The glass transition temperature (T_g) of bulk amorphous DACT-II (~6 mg) measured by conventional differential scanning calorimetry (DSC) at heating rates of 1–100 K min^{-1} was 151–159 °C. We also attempted DSC measurements for DACT-II in

vacuum-deposited amorphous thin films with a thickness of 100 nm (~20 ng). The ultrasensitive measurements were successful using very fast heating rates of 500–3,000 K s^{-1}, giving T_g of 192–197 °C. T_g of the thin films was higher than that of bulk samples, although it would be decreased by extrapolating to a lower heating rate. The higher T_g probably reflects the higher thermal stability of vacuum-deposited thin films than bulk samples[25] (Supplementary Note 3). DACT-II was then used as an emitting material for OLEDs (**DACT-II devices**). Supplementary Fig. 3 shows the materials for the devices; *N*,*N*′-di(naphthalen-1-yl)-*N*,*N*′-diphenyl-[1,1′-biphenyl]-4,4′-diamine (NPD) or 4,4′-(cyclohexane-1,1-diyl)bis(*N*,*N*-di-*p*-tolylaniline) (TAPC) was used for the hole-transport layer (HTL), ([1,1′-biphenyl]-4-yloxy)bis((2-methylquinolin-8-yl)oxy)aluminium (BAlq) or 3,3″,5,5″-tetra(pyridin-3-yl)-1,1′:3′,1″-terphenyl (BmPyPhB) for the electron-transport layer (ETL), lithium quinolin-8-olate (Liq) for the electron-injection layer (EIL) and 4,4′-di(9*H*-carbazol-9-yl)-1,1′-biphenyl (CBP) for the host material of the emitter layer (EML). The device structure was indium tin oxide (ITO)/HTL (100 nm)/EML (40 nm)/ETL (30 nm)/Liq/Al (Fig. 1d and Supplementary Fig. 4). CBP doped with *x* wt% DACT-II was used for the EML. The devices are termed **DACT-II-*x* devices**, where *x* corresponds to the respective wt% of DACT-II. Hereafter, the **DACT-II-*x* devices**, containing TAPC and BAlq as HTL and ETL, respectively, are discussed unless otherwise stated. The energy-level diagram of the devices is shown in Fig. 1d. A neat DACT-II layer was also used for the EML in the **DACT-II-100 device**. The results and band diagrams for devices containing NPD or BmPyPhB are included in Table 1, Supplementary Tables 1 and 2, and Supplementary Figs 4 and 5. Typical fluorescent and phosphorescent devices were also fabricated for reference using *mer* tris(8-hydroxyquinoline) aluminum(III) (Alq_3) and *fac* tris(2-phenylpyridine) iridium(III) ($Ir(ppy)_3$) as emitters, respectively. The structures of the **Alq_3 device** and **$Ir(ppy)_3$ device** are shown in Supplementary Fig. 4.

Figure 2a shows EL spectra of **DACT-II devices** at a current density of 1 mA cm^{-2}. The OLEDs, containing DACT-II concentrations of 1 to 23 wt%, all emit green EL. The emission maxima (λ_{max}) range from 516 to 537 nm, with a small red shift observed with increasing DACT-II concentration. λ_{max} of PL spectra has a stronger concentration dependence, as shown in Fig. 2b (see Supplementary Note 4). EL spectra with a logarithmic EL intensity scale are shown in Supplementary Fig. 6. The **DACT-II-1 device** contains emission from TAPC and/or CBP (Supplementary Figure 6 also shows the PL spectra of the respective materials). However, no obvious radiative emission from any other layer is detected for any of the other devices. This indicates that excitons are confined within the emission layer, despite the absence of blocking layers. In addition, no emission originating from CBP is observed, except for the **DACT-II-1 device**. This indicates that excitons are well-confined on DACT-II molecules, by direct charge injection and/or complete energy transfer from the CBP host. In Fig. 2c, EQE is shown as a function of luminance. The EQE for representative **DACT-II-*x* devices** are given in Table 1 (Data for all OLEDs without and with out-coupling sheets are listed in Supplementary Tables 1 and 2, respectively). The maximum EQE of 29.6% is obtained at 5 cd m^{-2} (5 μA cm^{-2}) for the **DACT-II-9 device** (filled black circles in Fig. 2c). EQEs of a typical fluorescent **Alq_3 device** and phosphorescent **$Ir(ppy)_3$ device** are also shown in Fig. 2c, as black dot-dashed and solid lines, respectively. Maximum EQEs of the **Alq_3** and **$Ir(ppy)_3$ devices** are 1.3% and 13.0%, respectively. Maximum EQEs of all fabricated **DACT-II devices** exceed those of the **Alq_3** and **$Ir(ppy)_3$ devices**, except for the **DACT-II-1 device**. EQE values of the **DACT-II-9 device** are extremely large, even at the luminance levels of practical applications; 22.8% at 500 cd m^{-2} (for display applications) and 16.2% at 3,000 cd m^{-2} (for lighting applications) (Table 1). Although EQE decreases with increasing luminance, the efficiency roll-off is overcome by increasing the concentration of DACT-II in the EML. Figure 2c and Table 1 show that EQE values of 26.9% and 21.8% are obtained at 500 cd m^{-2} and 3,000 cd m^{-2}, respectively, for the **DACT-II-19 device**.

Although the devices are relatively thick (Fig. 1d), the **DACT-II devices** exhibit low power consumption, especially at high DACT-II concentrations. The turn-on voltage (voltage at 1 cd m^{-2}) decreased with increasing DACT-II concentration and was 2.6 V for the **DACT-II-19 device**. This suggests that with increasing DACT-II concentration, charges tend to be injected directly into DACT-II molecules rather than via the CBP host, as supposed from Fig. 1d.

Photoluminescence quantum yield. We investigate the origin of the excellent EQE of DACT-II by first discussing the PLQY (Supplementary Note 5). The PLQY of DACT-II in toluene is 46.0%, which decreases to 26.6% on bubbling O_2 through the solution. Bubbling with Ar excludes O_2 and results in a PLQY of 63.7%. This suggests that some excitons, transferred to T_1 via ISC, are quenched by dissolved O_2 (refs 17,18). In the Ar-purged system, excitons in T_1 are not quenched and revert to S_1 through RISC, resulting in a higher PLQY. Phosphorescence can be discounted as demonstrated below. The PLQY of the neat film is only 43.6 ± 4%, but PLQY values of 101.1 ± 4% are obtained for the 9 wt% DACT-II-doped CBP thin films, when DACT-II is directly

Table 1 | EQE values for selected DACT-II-*x* devices.

Device	EQE (%)					
	Max	@1 cd m^{-2}	@10 cd m^{-2}	@100 cd m^{-2}	@500 cd m^{-2}	@3,000 cd m^{-2}
DACT-II-3	20.5	18.6	19.4	16.1	13.6	10.1
DACT-II-6	28.7	**27.9**	28.1	25.1	21.4	15.3
DACT-II-9	**29.6**	23.2	**29.2**	26.5	22.8	16.2
DACT-II-12	27.7	21.6	26.6	26.3	23.9	18.0
DACT-II-19	27.9	24.8	26.4	**27.9**	**26.9**	**21.8**
DACT-II-23	25.2	22.4	23.7	25.2	22.1	17.9
DACT-II-9*	**41.5**	**41.1**	**41.3**	37.9	32.9	24.7
DACT-II-9†	40.4	30.7	39.5	**39.9**	**37.6**	**30.7**

EQE, electroluminescence quantum efficiency; DACT-II, 9-[4-(4,6-diphenyl-1,3,5-triazin-2-yl)phenyl]-*N*,*N*,*N*′,*N*′-tetraphenyl-9*H*-carbazole-3,6-diamine.
*With out-coupling sheet.
†With out-coupling sheet, BmPyPhB was used as the ETL.
EQE values in bold are the maximum for respective luminances without and with out-coupling sheet.

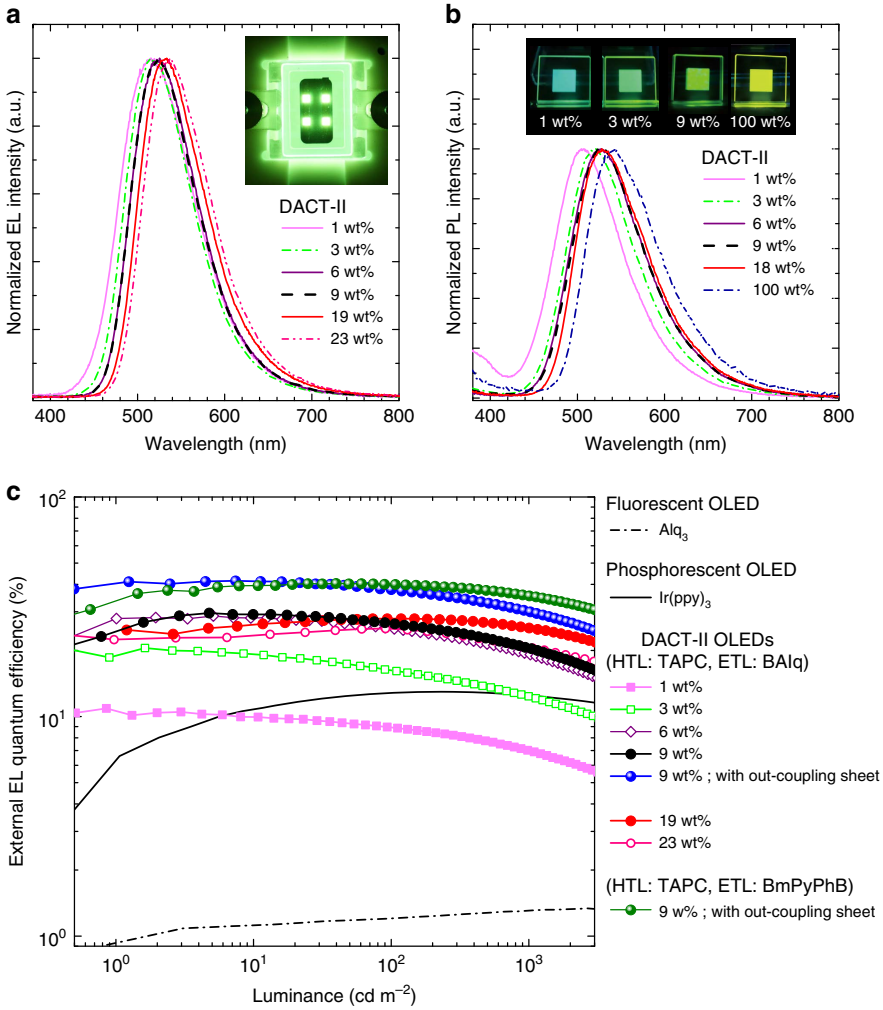

Figure 2 | EL and PL of DACT-II. (**a**) EL spectra for the **DACT-II-*x* devices**. A photograph of EL emission for the **DACT-II-9 device** is also shown. (**b**) PL spectra of DACT-II in CBP films and a neat DACT-II film. Photographs of PL emission are also shown. (**c**) EQE versus luminance for the **DACT-II-*x* devices**. EQE values of the **Alq_3 device** and **$Ir(ppy)_3$ device** are also shown.

excited. The PLQYs are 100.3 ± 4% for the 9 wt% doped films even when CBP is excited, indicating that all the excitons transfer from CBP to DACT-II without any loss (ultraviolet–visible spectra of DACT-II and CBP films are given in Supplementary Fig. 7).

Exciton generation factor. Another important factor influencing EQE is β, that is, the singlet/triplet branching ratio. In PL experiments, excitation produces excitons in S_1. Figure 3a shows the transient PL decay of DACT-II in toluene. When O_2 is removed by Ar bubbling, two components with prompt and delayed PL decays are observed. This differs from the result for the as-prepared solution containing O_2, in which only the prompt decay component is observed. The results indicate that the prompt decay arises from fluorescence directly from the S_1-to-S_0 transition. The delayed component arises from phosphorescence from T_1 via ISC, or delayed fluorescence from S_1 through ISC and subsequent RISC, because it is quenched by the O_2 triplet state in the presence of O_2 (refs 17,18). Continuous transitions between S_1 and T_1 are theoretically possible, but also result in either phosphorescence or delayed fluorescence.

Prompt and delayed PL decay components are also observed for thin films. Figure 3b shows the doping concentration dependence of the transient PL decays for DACT-II-doped CBP thin films (The temperature dependence is shown in Supplementary Fig. 8). Both prompt and delayed components are observed for all films, and the delayed component increases with increasing DACT-II concentration. Phosphorescence and delayed fluorescence are easily distinguished from the temperature dependence of the transient PL decay. Delayed fluorescence exhibits an increase in delayed emission with increasing temperature. Conversely, inverse temperature dependence is found in the case of phosphorescence. The intensity of the delayed component is absent at 10 K but gradually increases with increasing temperature (Supplementary Fig. 8), indicating that the delayed emission is thermally activated. Thus, the delayed component originates from TADF.

TTA is another possible origin of delayed fluorescence, which can also improve OLED efficiency[26–29]. However, β obtained by TTA is theoretically limited to 62.5%. The IQE, and therefore β, in this study reached 100% as clearly shown below, confirming that the delayed fluorescence originates from RISC.

The radiative rate constants for the prompt (k_p) and delayed (k_d) components, rate constants for ISC (k_{ISC}) and RISC (k_{RISC}), and total (Φ_{PL}) and fraction of delayed (Φ^d_{PL}) emission quantum yields are shown in Table 2 (see Supplementary Note 6 for the analysis). ΔE_{ST} determined from the Arrhenius plot of k_{RISC} is 9.0 meV (Fig. 3c). The currently reported TADF emitting material with the highest efficiency is the carbazolyldicyanobenzene derivative 4CzIPN[19], whose experimental ΔE_{ST} is 82.6 meV.

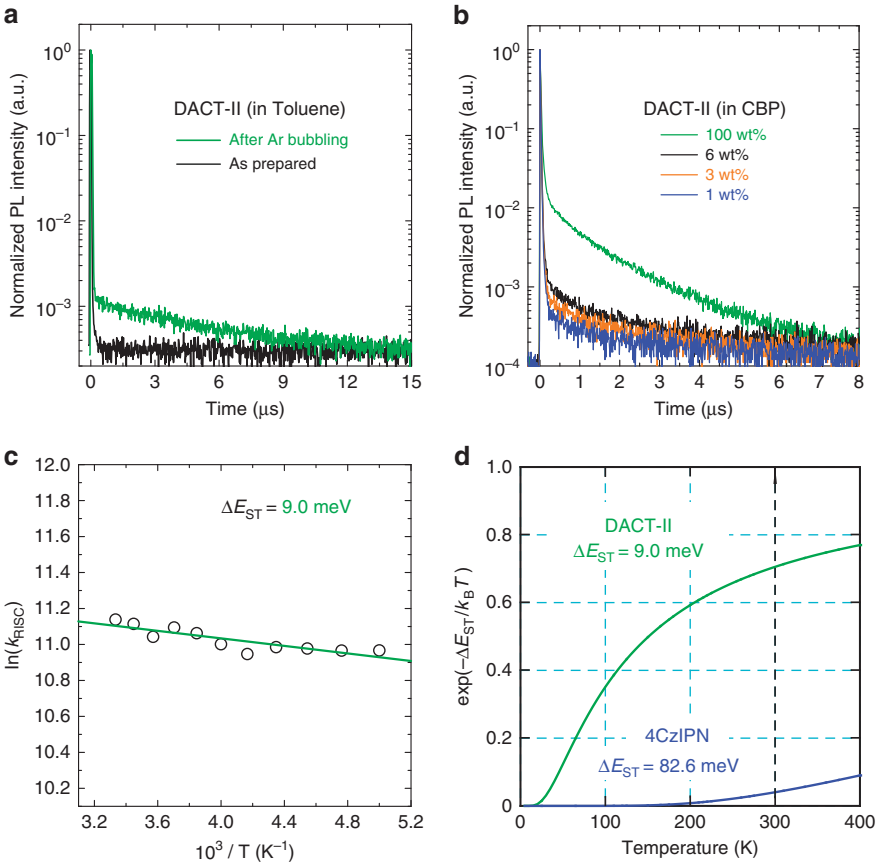

Figure 3 | TADF characteristics of DACT-II. (**a**) Transient PL decay characteristics of DACT-II in toluene at room temperature. (**b**) Doping concentration dependence of transient PL decay of DACT-II doped into CBP thin films at room temperature. (**c**) Arrhenius plot of the RISC rate constant (k_{RISC}). ΔE_{ST} of 9.0 meV was obtained from least-squares fitting (solid line). (**d**) Temperature dependence of Boltzmann factor $\exp\left(-\frac{\Delta E_{ST}}{k_B T}\right)$ for DACT-II ($\Delta E_{ST} = 9.0$ meV) and 4CzIPN ($\Delta E_{ST} = 82.6$ meV).

Table 2 | Temperature dependence of various rate constants and PLQYs for CBP films doped with 6 wt% DACT-II.

Temp (K)	k_p ($\times 10^8$ s^{-1})	k_d ($\times 10^4$ s^{-1})	k_{ISC} ($\times 10^6$ s^{-1})	k_{RISC} ($\times 10^4$ s^{-1})	Φ_{PL} (%)	Φ^d_{PL} (%)
200	1.15	5.33	9.18	5.79	97.7	5.7
210	1.16	5.32	9.25	5.79	98.2	6.2
220	1.15	5.39	9.16	5.86	98.4	6.4
230	1.18	5.43	9.39	5.90	98.8	6.8
240	1.15	5.22	9.21	5.68	99.1	7.1
250	1.17	5.52	9.32	5.99	99.6	7.5
260	1.15	5.87	9.21	6.38	99.7	7.7
270	1.16	6.06	9.23	6.58	100.0	8.0
280	1.15	5.75	9.17	6.25	100.0	8.0
290	1.15	6.18	9.17	6.71	100.5	8.4
300	1.16	6.33	9.23	6.88	100.3	8.3

CBP, 4,4′-di(9*H*-carbazol-9-yl)-1,1′-biphenyl; DACT-II, 9-[4-(4,6-diphenyl-1,3,5-triazin-2-yl)phenyl]-*N*,*N*,*N*′,*N*′-tetraphenyl-9*H*-carbazole-3,6-diamine; PLQY, photoluminescence quantum yield; ISC, intersystem crossing; RISC, reverse ISC.
k_p, k_d: radiative rate constants for prompt and delayed components, respectively.
k_{ISC}, k_{RISC}: rate constants for ISC and RISC, respectively.
Φ_{PL}, Φ^d_{PL}: PLQYs for total and delayed components, respectively.

ΔE_{ST} of DACT-II is markedly smaller, reflecting the temperature dependence of k_{RISC}.

ΔE_{ST} of DACT-II is smaller than the thermal energy at 300 K (25.9 meV). Figure 3d compares the temperature dependence of the Boltzmann factors, $\exp(-\Delta E_{ST}/k_B T)$, for DACT-II and 4CzIPN. The Boltzmann factor of DACT-II at 300 K is 0.71, much larger than that of 4CzIPN, 0.041. This indicates that RISC occurs more readily in DACT-II than 4CzIPN. The temperature dependence of the Boltzmann factors suggests effective up-conversion from T_1 to S_1 for DACT-II even at low temperature. This is supported by the total PLQY remaining at ~100% at lower temperatures, as shown in Table 2. T_1 excitons are more easily up-converted to S_1 at higher temperature. This is an advantage of DACT-II TADF systems over other TADF and phosphorescent systems, the latter two systems cannot exhibit high PLQY across a wide temperature range.

The PL spectra of the prompt and delayed PL decay components are shown in Supplementary Fig. 9. These spectra are indistinguishable within experimental error, irrespective of temperature. This supports the fact that the delayed component originates from TADF, not phosphorescence. In phosphorescent OLEDs, the energy corresponding to ΔE_{ST} is lost during ISC. Although this does not affect the quantum yield, such energy loss is avoided (or there is even an energy gain) during RISC in TADF systems by exploiting the thermal energy at room temperature. This results in lower power consumption.

Time-dependent density functional theory[30,31] (TD-DFT) calculations indicate that the torsion angle (α) between the donor and acceptor moieties affects the spatial overlap of the HOMO and LUMO (Supplementary Fig. 1, $\alpha = 0°$ for planar configuration and 90° for perpendicular configuration). The value of f decreases with increasing α, so precise control of f by adjusting α is important in designing highly luminescent TADF compounds. The value of f for DACT-II (0.2400) is higher than that for 4CzIPN (0.0708). S_0, T_1 and S_1 have energy minima at α of 48°, 85° and 89°, respectively. Subtracting the energy minimum of T_1 (at $\alpha = 85°$) from that of S_1 (at $\alpha = 89°$) gives a calculated ΔE_{ST} of 5.2 meV (using TD-DFT with the PBE0/6-31G(d) basis set[22,23]). This is smaller than the ΔE_{ST} of 11.3 meV calculated for 4CzIPN at the same level of theory. We realized both ~100% up-conversion from T_1 to S_1 and ~100% radiative emission, that is to say, 100% conversion from electricity to light, through the fine-tuning of ΔE_{ST} and f, by precisely controlling the overlap of the HOMO and LUMO distributions in DACT-II. In real OLEDs, the energy levels of S_1 and T_1 likely have distributions, and ΔE_{ST} may fluctuate. This is due to the distributions of conformations and environments of individual DACT-II molecules because they are in an amorphous state.

Orientation of transition dipole moment. The orientation of transition dipole moments of emitter molecules greatly affects out-coupling efficiency[32–35]. Here the orientation of DACT-II was quantified by two methods, variable angle spectroscopic ellipsometry (VASE)[36–38] and angular-dependent PL measurements[32,33,39,40] (Supplementary Note 7). Figure 4a shows the results of VASE measurements. The ordinary and extraordinary optical constants differ in the spectra, indicating that the orientation of DACT-II molecules is not random. Quantitative analysis indicates that DACT-II tends to be parallel to the substrate with an order parameter S of -0.32 ± 0.01. The result is confirmed by the angular-dependent PL measurements (Fig. 4b), which gave $S = -0.29 \pm 0.05$, agreeing well with the above VASE result.

Out-coupling and carrier balance ratio. We performed electrical and optical simulations[41–43] for the **DACT-II-9 device** (Supplementary Note 8). Electrical simulations revealed that the injected electrons and holes effectively recombine in the EML near the interface with the HTL. Figure 4c shows the results of optical simulations for the **DACT-II-9 device**. IQE = 100% and $S = -0.29$ were used for the simulation. The contributions of respective optical modes are given as a function of emission wavelengths. EQE can be calculated by integrating the fraction of out-coupled mode with respect to emission wavelengths with weighting of the PL intensity in Fig. 2b. Figure 4d shows the

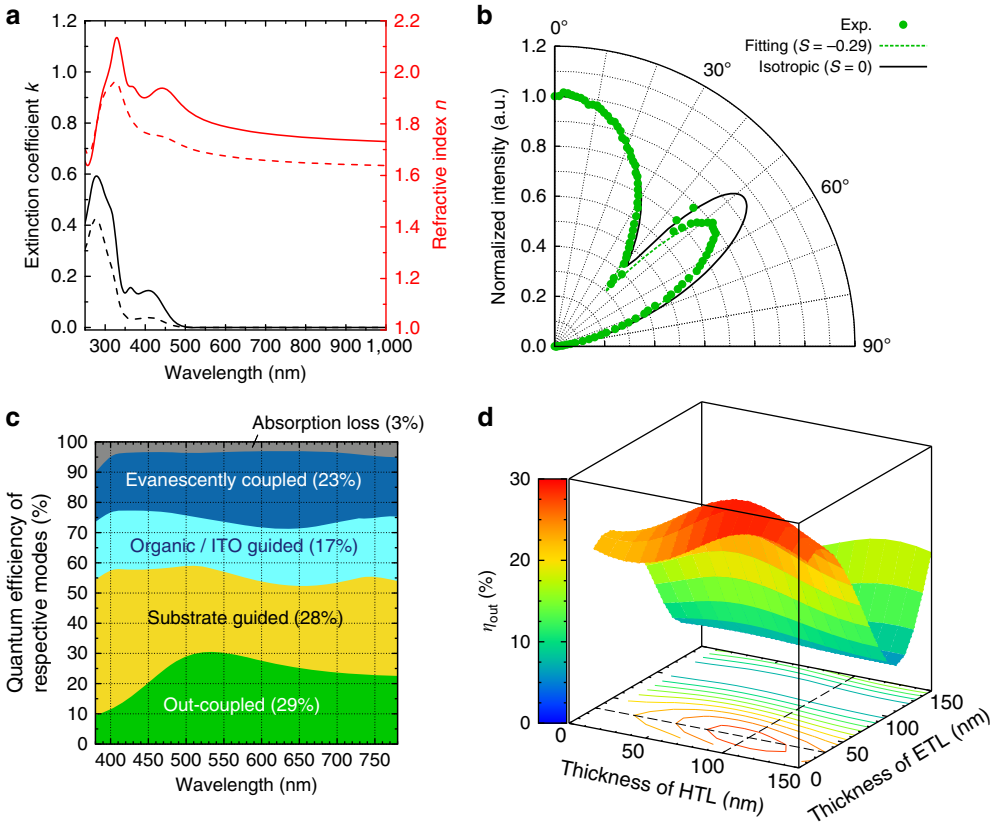

Figure 4 | Orientation of transition dipole moment and out-coupling. (**a**) Results of VASE measurements; extinction coefficient k (black) and refractive index n (red). The solid and dashed lines represent spectra for the ordinary and extraordinary optical constants, respectively. (**b**) Results of angular-dependent PL experiments. (**c**) Optical simulations for the **DACT-II-9 device**. The numbers in parentheses for respective modes are obtained by the integration with respect to emission wavelengths with weighting of the PL intensity. (**d**) Dependence of the out-coupling mode on the thicknesses of hole and electron-transport layers.

dependence of EQE on HTL and ETL thicknesses (see Supplementary Fig. 10 for all modes). The maximum EQE of 29.0 ± 0.9% was obtained for HTL and ETL thicknesses of 100 nm and 30 nm, respectively (for $S = -0.29 \pm 0.05$). The simulation results agree well with the experimental maximum EQE of 29.6%. The agreement clearly confirms the IQE ≈ 100%; that is, $\beta \approx \gamma \approx \Phi_{PL} \approx 100\%$ for the conditions of maximum EQE.

Thus far, we have made no effort to improve the out-coupling efficiency. The current OLEDs have a high $\eta_{out} = \eta_{EQE}/(\gamma \times \beta \times \Phi_{PL}) = 29.6/(1.0 \times 1.0 \times 1.0) = 29.6\%$. The IQE is already ~100%, so an increase in out-coupling efficiency is required to further increase EQE. Several methods have been reported to achieve this[44–48]. We opted for a simple, economical attachment of an out-coupling sheet to the OLED. Using an out-coupling sheet (Supplementary Fig. 11 and Supplementary Note 9) with a microlens array that also contained light-scattering particles yielded EQE values of 41.5% at maximum (filled blue circles in Fig. 2c), and 37.6% and 30.7% at 500 cd m^{-2} and 3,000 cd m^{-2}, respectively (filled green circles in Fig. 2c, see also Table 1 and Supplementary Table 2).

Discussion

We obtained a TADF material, DACT-II. OLEDs containing DACT-II have ~100% IQE, that is, 100% conversion from electricity to light. DACT-II has excellent thermal properties, and devices containing DACT-II are expected to perform well across a wide temperature range. By further optimizing device structures and surrounding materials, as seen for phosphorescent[11,49] and TADF-based[40] OLEDs, **DACT-II devices** are expected to deliver much higher performance, such as higher EQE at high luminance and lower power consumption. Improving the out-coupling efficiency will further increase the EQE of **DACT-II-based OLEDs**.

Methods

Summary of DACT-II synthesis. DACT-II was synthesized according to Supplementary Fig. 2 and Supplementary Note 2 with a 26% total yield. ^{1}H and ^{13}C nuclear magnetic resonance (NMR) spectra were recorded using JEOL ECA 600 MHz (Japan) and Bruker Avance III 800 MHz (Germany) spectrometers. DACT-II was purified by silica gel column chromatography using dichloromethane/hexane as an eluent, recrystallization and temperature-gradient sublimation.

Device fabrication and characterization. OLEDs with active areas of 4 mm^2 were fabricated by vacuum deposition at ~10^{-5} Pa on clean ITO-coated glass substrates with a deposition apparatus (SE-4260, ALS Technology, Japan). The deposition rates of HTL, EML, ETL, EIL, and Al were 0.1–0.2, 0.3–0.4, 0.1–0.2, 0.01, and 0.1–0.2 nm s^{-1}, respectively. After fabrication, devices were encapsulated with a glass cap using epoxy glue in a N_2-filled glove box. Calcium oxide was incorporated into the encapsulated package as a desiccant. OLED characteristics were measured with a source meter (2400, Keithley, Japan) and an absolute EQE measurement system (C9920-12, Hamamatsu Photonics, Japan). The integrating sphere for the measurements was calibrated before the experiments.

References

1. Bernanose, A., Comte, M. & Vouaux, P. A new method of emission of light by certain organic compounds. *J. Chim. Phys.* **50,** 64–68 (1953).
2. Bernanose, A. Electroluminescence of organic compounds. *Br. J. Appl. Phys.* **6,** S54–S56 (1955).
3. Pope, M., Kallmann, H. P. & Magnante, P. Electroluminescence in organic crystals. *J. Chem. Phys.* **38,** 2042–2043 (1963).
4. Tang, C. W. & VanSlyke, S. A. Organic electroluminescent diodes. *Appl. Phys. Lett.* **51,** 913–915 (1987).
5. Smith, L. H., Wasey, J. A. E. & Barnes, W. L. Light outcoupling efficiency of top-emitting organic light-emitting diodes. *Appl. Phys. Lett.* **84,** 2986–2988 (2004).
6. Chutinan, A., Ishihara, K., Asano, T., Fujita, M. & Noda, S. Theoretical analysis on light-extraction efficiency of organic light-emitting diodes using FDTD and mode-expansion methods. *Org. Electron.* **6,** 3–9 (2005).
7. Tanaka, D. *et al.* Ultra high efficiency green organic light-emitting devices. *Jpn J. Appl. Phys.* **46,** L10–L12 (2007).
8. Furno, M., Meerheim, R., Hofmann, S., Lüssem, B. & Leo, K. Efficiency and rate of spontaneous emission in organic electroluminescent devices. *Phys. Rev. B* **85,** 115205 (2012).
9. Baldo, M. A. *et al.* Highly efficient phosphorescent emission from organic electroluminescent devices. *Nature* **395,** 151–154 (1998).
10. Adachi, C., Baldo, M. A., Thompson, M. E. & Forrest, S. R. Nearly 100% internal phosphorescence efficiency in an organic light emitting device. *J. Appl. Phys.* **90,** 5048–5051 (2001).
11. Sasabe, H. & Kido, J. Recent progress in phosphorescent organic light-emitting devices. *Eur. J. Org. Chem.* **34,** 7653–7663 (2013).
12. Jablonski, A. Efficiency of anti-stokes fluorescence in dyes. *Nature* **131,** 839–840 (1933).
13. Jablonski, A. About the mechanism of photo-luminescence of dye phosphors. *Z. Physik.* **94,** 38–46 (1935).
14. Lewis, G. N., Lipkin, D. & Magel, T. T. Reversible photochemical processes in rigid media. A study of the phosphorescent state. *J. Am. Chem. Soc.* **63,** 3005–3018 (1941).
15. Parker, C. A. & Hatchard, C. G. Triplet-singlet emission in fluid solutions. Phosphorescence of eosin. *Trans. Faraday. Soc.* **57,** 1894–1904 (1961).
16. Parker, C. A. in *Advances Photochemistry,* Vol. 2 (eds Noyes, W. A., Hammond, G. S. & Pitts, J. N.) (John Wiley & Sons, Inc., Hoboken, NJ, USA, 1964).
17. Endo, A. *et al.* Efficient up-conversion of triplet excitons into a singlet state and its application to organic light emitting diodes. *Appl. Phys. Lett.* **98,** 0833022 (2011).
18. Méhes, G., Nomura, H., Zhang, O., Nakagawa, T. & Adachi, C. Enhanced electroluminescence efficiency in a spiro-acridine derivative through thermally activated delayed fluorescence. *Angew. Chem. Int. Ed.* **51,** 11311–11315 (2012).
19. Uoyama, H., Goushi, K., Shizu, K., Nomura, H. & Adachi, C. Highly efficient organic light-emitting diodes by delayed fluorescence. *Nature* **492,** 234–238 (2012).
20. Dias, F. B. *et al.* Triplet harvesting with 100% efficiency by way of thermally activated delayed fluorescence in charge transfer OLED emitters. *Adv. Mater.* **25,** 3707–3714 (2013).
21. Sato, K. *et al.* Organic luminescent molecule with energetically equivalent singlet and triplet excited states for organic light-emitting diodes. *Phys. Rev. Lett.* **110,** 247401 (2013).
22. Hariharan, P. C. & Pople, J. A. The influence of polarization functions on molecular orbital hydrogenation energies. *Theor. Chim. Acta* **28,** 213–222 (1973).
23. Adamo, C. & Barone, V. Toward reliable density functional methods without adjustable parameters: the PBE0 model. *J. Chem. Phys.* **110,** 6158–6170 (1999).
24. Frisch, M. J. *et al.* Gaussian 09, Revision C. 01. http://www.gaussian.com/index.htm (2010).
25. Swallen, S. F. *et al.* Organic glasses with exceptional thermodynamic and kinetic stability. *Science* **315,** 353–356 (2007).
26. Birks, J. B. *Photophysics of Aromatic Molecules.* 372 (Wiley-Interscience, 1970).
27. Kondakov, D. Y., Pawlik, T. D., Hatwar, T. K. & Spindler, J. P. Triplet annihilation exceeding spin statistical limit in highly efficient fluorescent organic light-emitting diodes. *J. Appl. Phys.* **106,** 124510 (2009).
28. Kohler, A. & Bässler, H. Triplet states in organic semiconductors. *Mater. Sci. Eng. R* **66,** 71–109 (2009).
29. Luo, Y. & Aziz, H. Correlation between triplet–triplet annihilation and electroluminescence efficiency in doped fluorescent organic light-emitting devices. *Adv. Funct. Mater.* **20,** 1285–1293 (2010).
30. Bauernschmitt, R. & Ahlrichs, R. Treatment of electronic excitations within the adiabatic approximation of time dependent density functional theory. *Chem. Phys. Lett.* **256,** 454–464 (1996).
31. Casida, M. E., Jamorski, C., Casida, K. C. & Salahub, D. R. Molecular excitation energies to high-lying bound states from time-dependent density-functional response theory: characterization and correction of the time-dependent local density approximation ionization threshold. *J. Chem. Phys.* **108,** 4439–4449 (1998).
32. Kim, S.-Y. *et al.* Organic light-emitting diodes with 30% external quantum efficiency based on a horizontally oriented emitter. *Adv. Funct. Mater.* **23,** 3896–3900 (2013).
33. Mayr, C. *et al.* Efficiency enhancement of organic light-emitting diodes incorporating a highly oriented thermally activated delayed fluorescence emitter. *Adv. Funct. Mater.* **24,** 5232–5239 (2014).
34. Schmidt, T. D., Scholz, B., Mayr, C. & Brütting, W. Efficiency analysis of organic light-emitting diodes based on optical simulations. *IEEE J. Sel. Top. Quantum Electron.* **19,** 7800412 (2013).
35. Schmidt, T. D. *et al.* Extracting the emitter orientation in organic light-emitting diodes from external quantum efficiency measurements. *Appl. Phys. Lett.* **105,** 043302 (2014).
36. Woollam, J. A. *et al.* Overview of variable angle spectroscopic ellipsometry (VASE), part I: basic theory and typical applications. *Proc. SPIE* **CR72,** 3–28 (1999).

37. Lin, H-W. *et al.* Anisotropic optical properties and molecular orientation in vacuum-deposited ter(9,9-diarylfluorene)s thin films using spectroscopic ellipsometry. *J. Appl. Phys.* **95,** 881–886 (2004).
38. Yokoyama, D., Setoguchi, Y., Sakaguchi, A., Suzuki, M. & Adachi, C. Orientation control of linear-shaped molecules in vacuum-deposited organic amorphous films and its effect on carrier mobilities. *Adv. Funct. Mater.* **20,** 386–391 (2010).
39. Frischeisen, J., Yokoyama, D., Adachi, C. & Brütting, W. Determination of molecular dipole orientation in doped fluorescent organic thin films by photoluminescence measurements. *Appl. Phys. Lett.* **96,** 073302 (2010).
40. Sun, J. W. *et al.* A fluorescent organic light-emitting diode with 30% external quantum efficiency. *Adv. Mater.* **26,** 5684–5688 (2014).
41. Knapp, E., Haeusermann, R., Schwarzenbach, H. U. & Ruhstaller, B. Numerical simulation of charge transport in disordered organic semiconductor devices. *J. Appl. Phys.* **108,** 054504 (2010).
42. Ruhstaller, B. *et al.* Simulating electronic and optical processes in multilayer organic light-emitting devices. *IEEE J. Sel. Top. Quantum Electron.* **9,** 723–731 (2003).
43. Perucco, B. *et al.* On the exciton profile in OLEDs-seamless optical and electrical modeling. *Org. Electron.* **13,** 1827–1835 (2012).
44. Jordan, R. H., Dodabalapur, A. & Slusher, R. E. Efficiency enhancement of microcavity organic light emitting diodes. *Appl. Phys. Lett.* **69,** 1997–1999 (1996).
45. Möller, S. & Forrest, S. R. Improved light out-coupling in organic light emitting diodes employing ordered microlens arrays. *J. Appl. Phys.* **91,** 3324–3327 (2002).
46. Sun, Y. & Forrest, S. R. Enhanced light out-coupling of organic light-emitting devices using embedded low-index grids. *Nat. Photon.* **2,** 483–487 (2008).
47. Reineke, S. *et al.* White organic light-emitting diodes with fluorescent tube efficiency. *Nature* **459,** 234–238 (2009).
48. Saxena, K., Jain, V. K. & Mehta, D. S. A review on the light extraction techniques in organic electroluminescent devices. *Opt. Mater.* **32,** 221–233 (2009).
49. Sasabe, H. *et al.* Extremely low operating voltage green phosphorescent organic light-emitting devices. *Adv. Funct. Mater.* **23,** 5550–5555 (2013).

Acknowledgements

This research was funded by the Japan Society for the Promotion of Science (JSPS) through the 'Funding Program for World-Leading Innovative R&D on Science and Technology (FIRST Program)', initiated by the Council for Science and Technology Policy (CSTP). This research was also supported by a Grant-in-Aid for Scientific Research (A) and by the Collaborative Research Program of Institute for Chemical Research, Kyoto University (grant # 2015- 14). Out-coupling sheets were kindly provided by Yuji Hotta, Optmate Corporation. Computation time on a supercomputer system was provided by the Institute for Chemical Research, Kyoto University, Japan, and the Academic Center for Computing and Media Studies (ACCMS), Kyoto University, Japan. NMR measurements were supported by the Joint Usage/Research Center (JURC) at the Institute for Chemical Research, Kyoto University, Japan.

Author contributions

H.K., K. Shizu and C.A. planned and supervised the project. K. Suzuki and H.O. performed the syntheses. H.K., T.F., A.W. and Y.M. supervised the syntheses. H.S. and T.F. fabricated devices and measured material and device performances. H.K. and T.F. supervised the device fabrication and characterization. K. Shizu and F.S. performed the theoretical calculations. S.K. performed the device simulation and H.K. supervised. T.K. and T.F. performed the VASE and angular-dependent PL measurements and H.K. supervised them. H.K., T.F., K. Shizu and K. Suzuki wrote the paper.

Additional information

Supplementary Information accompanies this paper at http://www.nature.com/naturecommunications

Competing financial interests: The authors declare no competing financial interests.

Reprints and permission information is available online at http://npg.nature.com/reprintsandpermissions/

How to cite this article: Kaji, H. *et al.* Purely organic electroluminescent material realizing 100% conversion from electricity to light. *Nat. Commun.* 6:8476 doi: 10.1038/ncomms9476 (2015).